CHEMISTRY
A EUROPEAN JOURNAL

DOI: 10.1002/chem.200903361

Highly Efficient Visible Light Plasmonic Photocatalyst Ag@Ag(Br,I)

Peng Wang,[a] Baibiao Huang,*[a] Qianqian Zhang,[b] Xiaoyang Zhang,[a] Xiaoyan Qin,[a] Ying Dai,[c] Jie Zhan,[a] Jiaoxian Yu,[a] Haixia Liu,[a] and Zaizhu Lou[a]

Abstract: The new plasmonic photocatalyst Ag@Ag(Br,I) was synthesized by the ion-exchange process between the silver bromide and potassium iodide, then by reducing some Ag^+ ions in the surface region of Ag(Br,I) particles to Ag^0 species. Ag nanoparticles are formed from Ag(Br,I) by the light-induced chemical reduction reaction. The Ag@Ag(Br,I) particles have irregular shapes with their sizes varying from 83 nm to 1 μm. The as-grown plasmonic photocatalyst shows strong absorption in the visible light region because of the plasmon resonance of Ag nanoparticles. The ability of this compound to reduce Cr^{VI} under visible light was compared with those of other reference photocatalyst. The plasmonic photocatalyst is shown to be highly efficient under visible light. The stability of the photocatalyst was examined by X-ray diffraction and X-ray photoelectron spectroscopy. The XRD pattern and XPS spectra prove the stability of the plasmonic photocatalyst Ag@Ag(Br,I).

Keywords: heterogeneous catalysis · photochemistry · plasmon photocatalysis · silver

Introduction

Since the conception of plasmonic photocatalyst was proposed,[1] the localized surface plasmon resonance (LSPR) effect of noble-metal nanoparticles on photocatalyst has been the focus of intense study.[2] The LSPR, an effect of the nanosize regime, is essentially light waves that are trapped on the surface due to the interaction with the free electrons of the metal.[3] Excitation of the conduction electrons occurs when there is resonance between the electrons and the oscillating electric field of the incident light, and this LSPR is observed as an extinction spectrum as light is passed through the sample. The spectral position of the LSPR and the scattering properties of metal nanoparticles depend on the sizes and shapes of the nanoparticles, compositions and dielectric constant of the surrounding medium.[4] The ability to fine-tune the LSPR properties has been a key factor in advancing and optimizing these applications in catalysis,[5] solar cell,[6] biological labeling,[7] optoelectronics,[8] photothermal cancer therapy,[9] and surface-enhanced Raman scattering.[10] Recently, we have explored new plasmonic photocatalyst Ag@AgBr,[11] which is highly efficiency in photooxidize methylic orange and stable under visible-light illumination, but the reducing ability of Ag@AgBr is poor. Generally speaking, the position of semiconductor's conduction band plays important role in the reducing ability. The position of the conduction band is higher, the reducing ability is stronger. By the same method as described in our early report,[12] we have determined the conduction band position of AgBr can be driven up by introduction of the iodine element. The conduction bands of AgBr and Ag(Br,I) are about −3.28 and −3.2679 eV. From the results of the calculation, we can predict that the reducing ability of Ag(Br,I) is stronger than that of AgBr. The reducing ability is checked by reducing of Cr^{VI}.

Chromium is widely used in industry and has resulted in a tremendous contamination.[13] In the environment, chromium is widely distributed and exists in two common oxidation states, Cr^{III} and Cr^{VI}.[14] Cr^{VI}, a carcinogen and mutagen, is mobile in both aqueous and subsurface environments, which is acutely toxic to most living organisms. In contrast to Cr^{VI}, the toxicity of Cr^{III} is relatively lower, which can be easily absorbed into a variety of inorganic and organic materials at neutral pH.[15] Furthermore, the trivalent chromium can be isolated as insoluble Cr^{III} hydroxides by adjusting the pH to

[a] P. Wang, Prof. Dr. B. Huang, Prof. X. Zhang, X. Qin, Prof. Dr. J. Zhan, J. Yu, H. Liu, Z. Lou
State Key Lab of Crystal Materials, Shandong University
Jinan 250100 (China)
E-mail: bbhuang@sdu.edu.cn

[b] Q. Zhang
School of Chemistry and Chemical Engineering
Shandong University, Jinan 250100 (China)

[c] Prof. Dr. Y. Dai
School of Physics, Shandong University
Jinan 250100 (China)

sufficiently high values, enabling the removal of chromium from the environment. Therefore, Cr^{VI} is usually reduced to Cr^{III} in order to minimize environmental pollution.[16] Cr^{VI} can be reduced to Cr^{III} by direct chemical reducing, using Fe^{II}/Fe^{III} and other biological methods.[17] Moreover, it can also be realized by photocatalytic reduction.[18]

TiO_2 has been investigated extensively in the fields of photocatalytic reduction of Cr^{VI}. As a photocatalyst, the TiO_2 suffers severe constraints in practical applications due to the wide band-gap (i.e., 3.2 eV for anatase and 3.0 eV for rutile; and hence can only be excited under the irradiation of UV light) and bottleneck of poor quantum yield that is normally caused by the rapid recombination of photogenerated electrons and holes. Since UV light corresponds to only 4% of the sunlight, a more efficient and visible light photocatalyst[19] is needed for reducing the pollution of Cr^{VI} brought by industry.

In the present report, we describe the synthesis and characterization of another analogous plasmonic photocatalyst Ag@Ag(Br,I), which has strong photoreducing ability. The reducing ability of the plasmonic photocatalysts (photogenerated electrons, reducing Cr^{VI}) has been checked. The plasmonic photocatalyst Ag@Ag(Br,I) is shown to be highly efficient in photoreduction of Cr^{VI} than that of Ag@AgBr. Our results have explored the usage of the photogenerated electrons, and have proved that the introducing iodine element can be used to enhance the reducing ability of the plasmonic photocatalyst Ag@AgBr.

Results and Discussion

The size and morphology of plasmonic photocatalyst Ag@Ag(Br,I) are depending on the size and morphology of the starting material Ag_2MoO_4. XRD analysis was carried out to investigate the crystal structure of the as-obtained Ag_2MoO_4. The typical XRD pattern of the Ag_2MoO_4 is given in Figure 1a. All the diffraction peaks could be indexed as the cubic phase (space group $Fd\bar{3}m$) of Ag_2MoO_4 with lattice constant $a=926$ Å (JCPDS Card No 75-250). No characteristic peaks belonging to other impurities were detected, indicating the synthesis of pure precursors.

The morphology and size of the starting material were investigated by SEM. Figure 1c shows the typical image of Ag_2MoO_4 with a size distribution (0.65–5 μm).

In Figure 1, some Ag_2MoO_4 appear as cobblestone-like submicron particles, and others appear as polyhedron-like particles, exposing more than four crystal faces.

The AgBr were fabricated by the ion-exchange process between Ag_2MoO_4 and HBr. The morphology of AgBr was determined by the Ag_2MoO_4. After the synthesis of the AgBr, the ion-exchange process between AgBr and KI resulted in the formation of Ag(Br,I).

The Ag(Br,I) solids were then added to a solution of MO dye, which was irradiated with a 300 W Xe arc lamp equipped with an ultraviolet cutoff filter to provide visible light with $\lambda \geq 400$ nm. Then the resulting precipitates, which consisted of silver NPs and Ag(Br,I) particles, were washed and dried in air. The crystal structures of the Ag@Ag(Br,I) samples were examined by XRD.

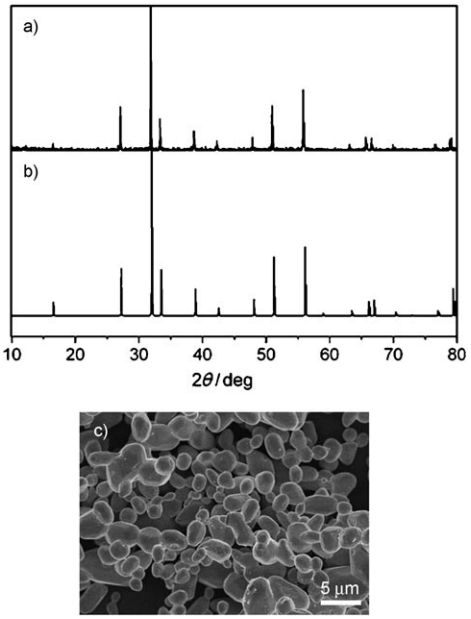

Figure 1. a) XRD pattern of the as prepared Ag_2MoO_4 sample; b) the standard Ag_2MoO_4 XRD pattern (JCPDS file 75-250); c) The typical SEM image of Ag_2MoO_4 sample.

The XRD pattern of the obtained Ag@Ag(Br,I) product is shown in Figure 2. Figure 2a can be indexed to the cubic phase of Ag with lattice constant $a=4.0861$ Å (JCPDS file: 65-2871) coexisting with Ag(Br,I) (JCPDS file: 48-1237).

The elemental compositions, chemical status and silver's content of Ag@Ag(Br,I) were also examined by X-ray photoelectron spectroscopy (XPS). Before the visible light irradiation, XPS results indicate that the Ag@Ag(Br,I) contains Ag, Br, I and C. The C element is due to the adventitious hydrocarbon from the XPS instrument itself. Ag, Cl and Br peaks are from the obtained Ag@Ag(Br,I) samples. Figures 3 and 4 show the XPS results of Ag@Ag(Br,I). The binding energies in the XPS spectra presented are calibrated

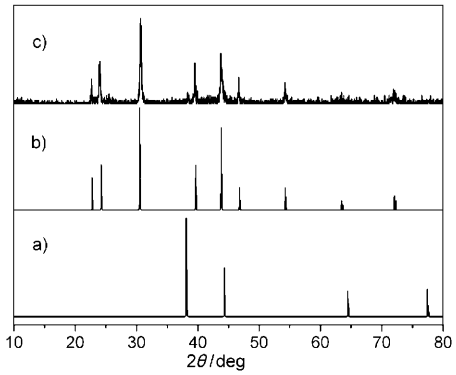

Figure 2. XRD patterns of a) Ag (JCPDS file: 65-2871), b) Ag(Br,I) (JCPDS file: 48-1237), c) the as prepared Ag@Ag(Br,I) sample.

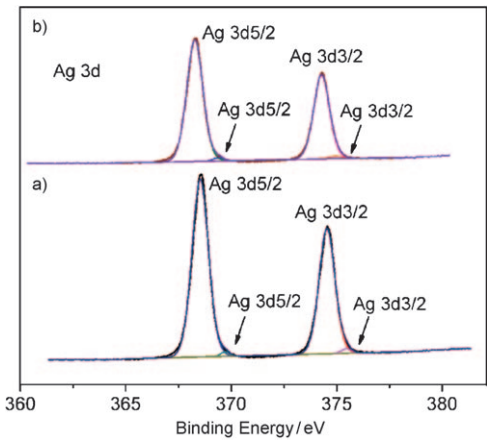

Figure 3. XPS spectra of a) Ag 3d of Ag@Ag(Br,I); b) Ag 3d of the corresponding Ag@Ag(Br,I) after 10 h irradiation under visible-light irradiation.

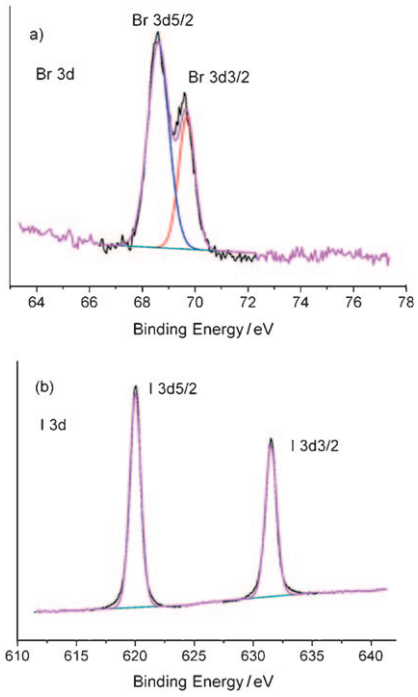

Figure 4. XPS spectra of a) Br 3d and b) I 3d of the obtained Ag@Ag(Br,I) sample.

by C1s (284.8 eV). In Figure 3 a, the Ag 3d spectra of Ag@Ag(Br,I) consists of two individual peaks at about 374 and 368 eV, which can be attributed to Ag 3d3/2 and Ag 3d5/2 binding energies, respectively. The Ag 3d3/2 and Ag 3d5/2 peak can be further divided into two different peaks at 374.54, 375.46 eV, and 368.53, 369.72 eV, respectively. And the peaks at 375.46 and 369.72 eV attribute to metal Ag^0 while the peaks at 368.53 and 374.54 eV attribute to Ag^I (Ag@Ag(Br,I)). The calculated surface Ag^0 content of the corresponding samples is 0.98 % (mol %), and the calculated surface Ag^+ content is 54.86 % (mol %). The spectra of Br 3d and I 3d are shown in Figure 4, the binding energies of Br 3d3 and 3d5 are −69.69 and −68.61 eV, and the binding energies of I 3d3 and 3d5 are −631.51 and −620.00 eV. The calculated Br and I contents are 12.76 % (mol %) and 31.41 % (mol %), respectively.

The scanning electron microscopy (SEM) image of Figure 5 shows the morphology of the as-prepared Ag@Ag(Br,I) sample. Compared with the precursor Ag_2MoO_4, the size of the Ag@Ag(Br,I) particles is smaller. It seems that the large particles of the Ag_2MoO_4 become into one more small nanoparticles. The Ag@Ag(Br,I) particles are in irregular shapes and their sizes vary from 83 nm to 1 μm. It is difficult to confirm the position and the size of the Ag nanoparticles. Higher resolution images can not be achieved because AgBr is decomposed by the high energy electron beam.

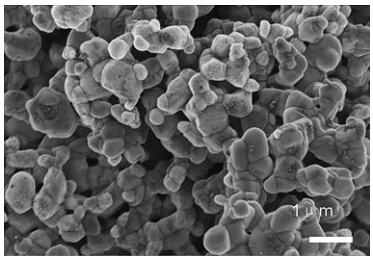

Figure 5. SEM image of Ag@Ag(Br,I) sample.

The UV/Vis diffuse reflectance spectra of Ag@Ag(Br,I) is presented in Figure 6. The Ag@Ag(Br,I) has stronger absorption in UV region than Ag@AgBr. Due to the plasmon resonance of Ag nanoparticles in the samples, both the plasmonic photocatalysts Ag@Ag(Br,I) and Ag@AgBr exhibit strong absorption in the visible region.

It was generally believed that Cr^{VI} could be reduced to Cr^{III} by the photogenerated electrons of TiO_2,[20] and the mechanism was reported in many works.[21] Figure 7 a shows the photocatalytic reduction of Cr^{VI} over plasmonic photocatalyst Ag@Ag(Br,I), which exhibits a high photcatalytic activity for Cr^{VI} reduction under visible light. It could be

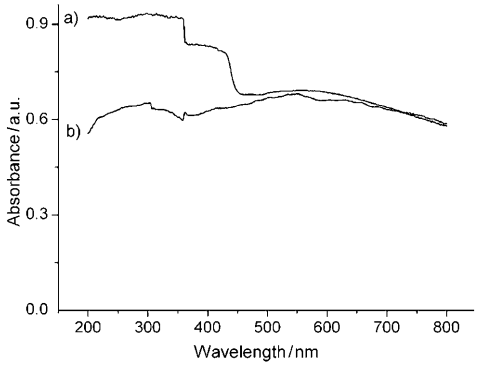

Figure 6. UV/Vis diffuse reflectance spectra of a) Ag@Ag(Br,I) and b) Ag@AgBr.

seen that the concentration of Cr^{VI} decreased with increasing irradiation time and nearly half the amount of Cr^{VI} is photocatalytically reduced after 20 min of irradiation, and almost all of the Cr^{VI} is reduced after 40 min of irradiation. Figure 7b shows the photocatalytic reduction of Cr^{VI} over Ag@Ag(Br,I) and Ag@AgBr. The results indicated that the rate of Cr^{VI} reduction with the Ag@Ag(Br,I) as a photocatalyst was faster than that with Ag@AgBr. Provided that the Cr^{VI} reduction reaction follows a pseudo-first order reaction, the rates of the Cr^{VI} decay over Ag@Ag(Br,I) and Ag@AgBr are estimated to be about 0.0356 and 0.004 mg min^{-1}. The rate for reduction of Cr^{VI} with Ag@Ag(Br,I) as a photocatalyst is around eight times as fast as that with Ag@AgBr. The blank experiment in the absence of the photocatalyst but under visible light irradiation and blank experiment using Ag@Ag(Br,I) and Ag@AgBr as the photocatalysts without irradiation were also done and the results demonstrated that the decay of Cr^{VI} was caused by the photocatalyst's reducing process.

The photooxidation capability of the plasmonic photocatalyst Ag@Ag(Br,I) sample was also evaluated by measuring the decomposition of methylic orange (MO) dye in the MO solution (with concentration of 20 mg L)$^{-1}$ under visible-light irradiation ($\lambda \geq 400$ nm). The degradation process is completed in about 35 min of visible-light irradiation, the rate of MO degradation over Ag@Ag(Br,I) is lower than that over Ag@AgBr. In the presence of different pollutants, the reaction groups are different. In the present of Cr^{VI}, the reaction group is photogenerated electrons, and the reduction ability of the electrons was determined by the position of semiconductor's conduction band, because the conduction band of Ag(Br,I) is higher than that of AgBr, (−3.2679 and −3.28 eV), so the reducing ability of Ag(Br,I) is stronger than that of AgBr; while in present of MO, the reaction group is photogenerated holes, and the oxidation of holes in AgBr is higher than that of Ag(Br,I).

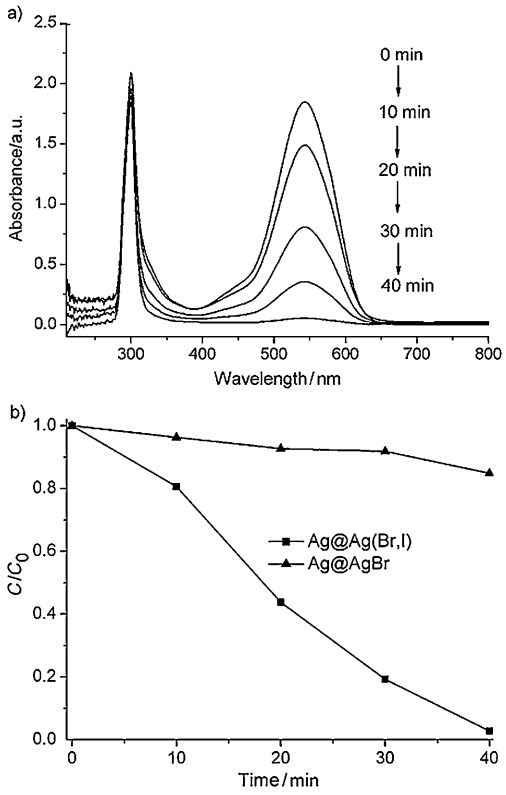

Figure 7. a) Changing UV/Vis spectrum of the aqueous solution in the presence of Ag@Ag(Br,I) under visible light irradiation (using diphenycarbazide as a developer at 540 nm). b) Photocatalytic reduction of Cr^{VI} in a slurry system over plasmonic photocatalysts Ag@Ag(Br,I) (■) and Ag@AgBr (▲) under visible-light irradiation ($\lambda \geq 400$ nm). *c* is the concentration of Cr^{VI} at time t, and C_0 that in the slurry system immediately after it is kept in the dark to obtain equilibrium adsorption state.

The photocatalystic results have proved that the plasmonic photocatalyst Ag@Ag(Br,I) can be used to reduce the Cr^{VI} and decompose the organic pollution (MO). Due to the plasmon resonance of Ag nanoparticles, the plasmonic photocatalyst shows great absorption in visible light region. After excited by the light, the photogenerated electron-hole pairs appear in the system. During the process of the decay of Cr^{VI}, the photogenerated electrons correspond to the reduction of Cr^{VI}. And the photogenerated holes are expected to be trapped by EDTA.[21a] During the process of the destruction of the MO, the photogenerated holes transfer to the surface of the system correspond to the oxidation of MO dye. And the photogenerated electrons are expected to be trapped by O_2 in the solution to form superoxide ions and other reactive oxygen species.[22] The outstanding photocatalytic activities of the plasmonic photocatalyst are related to the size of the particles, high adsorption of visible light, and effective separation of the photogenerated electrons and holes. The good surface contact of Ag metal particles to the Ag(Br,I) matrix also takes an important role, playing the function of metal-semiconductor heterojunctions, enhancing the charge transfer, and hence improving the photocatalysis efficiency.[23]

The photostability is very important for the plasmonic photocatalyst's application. Thus, the stability of plasmon photocatalyst Ag@Ag(Br,I) is further investigated. The Ag@Ag(Br,I) photocatalyst has been put under the irradiation of visible light for 10 h, and the XRD and XPS have been taken to check the photostability (10 h is long enough to achieve five turns of the photoreduction of hexavalent chromium and photooxidation of MO). The XRD pattern of the Ag@Ag(Br,I) after visible light irradiation of 10 h is almost identical to that of the as-prepared sample with the cubic phase of Ag (JCPDS file: 65-2871) coexists with the cubic phase of Ag(Br,I) (JCPDS file: 48-1237) (not shown here). The XPS spectra of photocatalyst Ag@Ag(Br,I) after visible light irradiation of 10 h is shown in Figure 3b, and the calculated surface Ag content of the corresponding samples is 1.17% (mol%). The calculated surface Ag^+, Br and I contents are 54.41% (mol%), 12.89% (mol%) and 31.53% (mol%), respectively. The content hardly changes. Therefore, it's considered that the Ag@Ag(Br,I) plasmonic photocatalyst in our experiment conditions is highly efficient and stable under visible-light irradiation.

Conclusion

The plasmonic photocatalyst Ag@Ag(Br,I) has been fabricated by the ion-exchange process and light-induced chemical reduction reaction. The photocatalyst has strong absorption in the visible region for the plasmon resonance of Ag nanoparticles. By introducing the iodine element, the plasmonic photocatalyst Ag@Ag(Br,I) exhibites superior photocatalytic activity for the reduction of Cr^{VI} under visible light irradiation than Ag@AgBr photocatalyst. The XRD pattern and XPS spectra results proved the stability of the plasmonic photocatalyst Ag@Ag(Br,I). Our studies suggest that the plasmonic photocatalyst Ag@Ag(Br,I) active in visible light can be widely used in the photoreduction of heavy metal (hexavalent chromium) and photooxidation of organic pollution (MO).

Experimental Section

Materials: Silver nitrate, potassium iodide, perchloric acid and diphenylcarbazide were purchased from Statepharm Chemical Reagent. Co. Ltd. (Shanghai) and hydrochloric acid was purchased from Kang de Chemical Reagent. Co. Ltd. (Shandong); Sodium molybdate, sodium hydroxide, hydrobromic acid and potassium chromate were purchased from Kemel Chemical Reagent. Co. Ltd. (Tianjing). All reagents were used as received without further treatment.

Preparation of silver molybdate: The silver molybdate was synthesized as previously described.[1b] A 0.2 M $AgNO_3$ solution (10 mL) was mixed with 0.1 M Na_2MoO_4 solution (10 mL), without adjusting the pH value of the mixed solution. The resulting solution was stirred for about 0.5 h, transferred to a special Teflon autoclave, and then heated at 180 °C for 1 h under microwave irradiation, which led to precipitation of Ag_2MoO_4. The Ag_2MoO_4 precipitates were collected, washed with deionized water until the pH value of the washing solution was about 7, and dried in air at 80 °C for 8 h.

AgBr was synthesized by the ion-exchange reaction between Ag_2MoO_4 and HBr. Ag_2MoO_4 was sonicated in concentrated HBr until completion of the ion-exchange process. This process yielded H_2MoO_4, which was dissolved in an excess of HBr. AgBr were precipitated. The AgBr precipitates were collected, washed with deionized water and dried in air.

Preparation of Ag(Br,I): AgBr (1.878 g) was added into the reaction vessel, which contained KI solution (100 mL, 0.05 mol L^{-1}). The vessel was stirred for about 3–5 d. Then Ag(Br,I) precipitates were collected, washed with deionized water and dried in air.

The obtained Ag(Br,I) powders were put into a solution of MO dye, which were then irradiated with a 300 W Xe arc lamp equipped with an ultraviolet cutoff filter to provide visible light with $\lambda \geq 400$ nm. Then the resulting precipitates, which consisted of silver NPs and Ag(Br,I) particles, were washed and dried in air.

The crystal structure of the sample was examined by X-ray diffraction (XRD, Bruker AXS D8), it's morphology by Scanning Electron Microscopy (SEM, Hitachi S-4800 microscopy), and diffuse reflectance by UV/Vis spectroscopy (UV-2550, Shimadzu). The content of Ag element in Ag@Ag(Br,I) photocatalyst was confirmed by X-ray photoelectron spectroscopy measurements (VG MicroTech ESCA 3000 X-ray photoelectron spectroscope using monochromatic $A1_{K\alpha}$ with a photon energy of 1486.6 eV at a pressure of $>1\times10^{-9}$ Torr, a pass energy of 40 eV, an electron takeoff angle of 60 °C, and an overall resolution of 0.05 eV). The XPS spectra were fitted using a combined polynomial and Shirley-type background function. The activities of the photocatalysts were evaluated by studying the reduction of Cr^{VI}. The reduction of the Cr^{VI} was carried out with the powdered Ag@Ag(Br,I) photocatalyst (0.1 g) suspended in a solution of K_2CrO_4 (100 mL, 14.24 mg L^{-1}). The pH of the reaction suspension was adjusted to 2 with diluted $HClO_4$, and EDTA was also added as sacrificial reagent. After the photocatalytic experiment was started by the irradiation of visible light, 5 mL volume of solution were periodically withdrawn from the reaction vessel, and the Cr^{VI} concentrations were measured using the diphenycarbazide (DPC) method at 540 nm[24] on a UV/Vis spectrophotometer (UV-7502PC, Xinmao, Shanghai). The optical system for detecting the catalytic reaction included a 300 W Xe arc lamp (PLS-SXE300, Beijing Trusttech Co. Ltd) with UV cutoff filter (providing visible light $\lambda \geq 400$ nm).

Acknowledgements

This work was financially supported by the National Basic Research Program of China (973 Program, Grant 2007CB613302), the National Natural Science Foundationof China under Grant 20973102, 50721002, and 10774091.

[1] a) K. Awazu, M. Fujimaki, C. Rockstuhl, J. Tominaga, H. Murakami, Y. Ohki, N. Yoshida, T. Watanabe, *J. Am. Chem. Soc.* **2008**, *130*, 1676–1680; b) P. Wang, B. B. Huang, X. Y. Qin, X. Y. Zhang, Y. Dai, J. Y. Wei, M. H. Whangbo, *Angew. Chem.* **2008**, *120*, 8049–8051; *Angew. Chem. Int. Ed.* **2008**, *47*, 7931–7933.

[2] X. Chen, H. Y. Zhu, J. C. Zhao, Z. F. Zheng, X. P. Gao, *Angew. Chem.* **2008**, *120*, 5433–5436; *Angew. Chem. Int. Ed.* **2008**, *47*, 5353–5356.

[3] P. K. Jain, X. Huang, I. H. El-Sayed, M. A. El-Sayed, *Plasmonics* **2007**, *2*, 107–118.

[4] a) W. A. Murray, W. L. Barnes, *Adv. Mater.* **2007**, *19*, 3771–3782; b) J. Perez-Juste, I. Pastoriza-Santos, L. M. Liz-Marzan, P. Mulvaney, *Chem. Rev.* **2005**, *105*, 1870–1901; c) S. Link, M. B. Mohamed, M. A. El-Sayed, *J. Phys. Chem. B* **1999**, *103*, 3073–3077; d) C. Wu, Q.-H. Xu, *Langmuir* **2009**, *25*, 9441–9446.

[5] a) E. Formo, E. Lee, D. Campbell, Y. Xia, *Nano Lett.* **2008**, *8*, 668–672; b) H. Song, R. M. Rioux, J. D. Hoefelmeyer, R. Komor, K. Niesz, M. Grass, P. Yang, G. A. Somorjai, *J. Am. Chem. Soc.* **2006**, *128*, 3027–3037; c) J. G. Yu, G. P. Dai, B. B. Huang, *J. Phys. Chem. C* **2009**, *113*, 16394–16401; d) C. Hu, T. W. Peng, X. X. Hu, Y. L. Nie, X. F. Zhou, J. H. Qu, H. He, *J. Am. Chem. Soc.* **2010**, *132*, 857–862.

[6] a) R. A. Pala, J. White, E. Barnard, J. Liu, M. L. Brongersma, *Adv. Mater.* **2009**, *21*, 3504–3509; b) T. Kume, S. Hayashi, H. Ohkuma, K. Yamamoto, *Jpn. J. Appl. Phys. Part 1* **1995**, *34*, 6448; c) O. Stenzel, A. Stendal, K. Voigtsberger, C. von Borczyskowski, *Sol. Energy Mater. Sol. Cells* **1995**, *37*, 337–348; d) S. D. Standridge, G. C. Schatz, J. T. Hupp, *J. Am. Chem. Soc.* **2009**, *131*, 8407–8409.

[7] a) S. R. Nicewarner-Pena, R. G. Freeman, B. D. Reiss, L. He, D. J. Pena, I. D. Walton, R. Cromer, C. D. Keating, M. J. Natan, *Science* **2001**, *294*, 137–141; b) N. L. Rosi, D. A. Giljohann, C. S. Thaxton, A. K. R. Lytton-Jean, M. S. Han, C. A. Mirkin, *Science* **2006**, *312*, 1027–1030.

[8] a) H. Xu, E. J. Bjernel, M. Kall, L. Borjesson, *Phys. Rev. Lett.* **1999**, *83*, 4357–4360; b) L. Polavarapu, N. Venkatram, W. Ji, Q.-H. Xu, *ACS Appl. Mater. Interfaces* **2009**, *1*, 2298–2303; c) X. M. Lu, M. S. Yavuz, H. Y. Tuan, B. A. Korgel, Y. N. Xia, *J. Am. Chem. Soc.* **2008**, *130*, 8900–8901; d) M. K. Kwon, J. Y. Kim, B. H. Kim, I. K. Park, C. Y. Cho, C. C. Byeon, S. J. Park, *Adv. Mater.* **2008**, *20*, 1253–1257.

[9] a) S. E. Skrabalak, J. Chen, L. Au, X. Lu, X. Li, Y. Xia, *Adv. Mater.* **2007**, *19*, 3177–3184; b) A. M. Gobin, M. H. Lee, N. J. Halas, W. D. James, R. A. Drevek, J. L. West, *Nano Lett.* **2007**, *7*, 1929–1934; c) J. Chen, D. Wang, J. Xi, L. Au, A. Siekkinen, A. Warsen, Z.-Y. Li, H. Zhang, Y. Xia, X. Li, *Nano Lett.* **2007**, *7*, 1318–1322.

[10] a) S. Nie, S. R. Emory, *Science* **1997**, *275*, 1102–1106; b) M. Rycenga, J. M. McLellan, Y. Xia, *Adv. Mater.* **2008**, *20*, 2416–2420.

[11] P. Wang, B. B. Huang, X. Y. Zhang, X. Y. Qin, H. Jin, Y. Dai, Z. Y. Wang, J. Y. Wei, J. Zhan, S. Y. Wang, J. P. Wang, M.-H. Whangbo, *Chem. Eur. J.* **2009**, *15*, 1821–1824.

[12] P. Wang, B. B. Huang, X. Y. Zhang, X. Y. Qin, Y. Dai, H. Jin, J. Y. Wei, M.-H. Whangbo, *Chem. Eur. J.* **2008**, *14*, 10543–10546.
[13] a) C. L. Hsu, S. L. Wang, Y. M. Zou, *Environ. Sci. Technol.* **2007**, *41*, 7907–7914b) B. Sun, E. Reddy, P. Smirniotis, *Environ. Sci. Technol.* **2005**, *39*, 6251–6259; c) M. Ding, X. Shi, *Mol. Cell. Biochem.* **2002**, *234*, 293–300.
[14] J. Kotas, Z. Stasicka, *Environ. Pollut.* **2000**, *107*, 263–283.
[15] S. Srivastava, S. Prakash, M. M. Srivastava, *Biometals* **1999**, *12*, 201–207.
[16] a) *Natural Attenuation of Hexavalent Chromium in Groundwater and Soils* (Eds.: C. D. Palmer, R. W. Puls), Superfund Technology Support Center for Ground Water, Robert S. Kerr Environmental Research Laboratory, **1994**, p. 12; b) *Chromium in the Natural and Human Environments, Vol. 20* (Ed.: J. O. Nriagu), Wiley, New York, **1988**.
[17] a) S. Pamukcu, A. Weeks, J. K. Wittle, *Environ. Sci. Technol.* **2004**, *38*, 1236–1241; b) L. Legrand, A. E. Figuigui, F. Mercier, A. Chausse, *Environ. Sci. Technol.* **2004**, *38*, 4587–4595; c) S. J. Hug, H. Laubscher, B. R. James, *Environ. Sci. Technol.* **1997**, *31*, 160–170; d) I. J. Buerge, S. J. Hug, *Environ. Sci. Technol.* **1998**, *32*, 2092–2099.
[18] a) H. B. Yu, S. Chen, X. Quan, H. M. Zhao, Y. B. Zhang, *Environ. Sci. Technol.* **2008**, *42*, 3791–3796; b) M. Gaberell, Y. P. Chin, S. J. Hug, B. Sulzberger, *Environ. Sci. Technol.* **2003**, *37*, 4403–4409; c) J. J. Testa, M. A. Grela, M. I. Litter, *Environ. Sci. Technol.* **2004**, *38*, 1589–1594; d) J. A. Navío, G. Colon, M. Trillas, J. Peral, *Appl. Catal. B* **1998**, *16*, 187–196.
[19] a) G. Liu, L. Z. Wang, C. H. Sun, Z. G. Chen, X. X. Yan, L. Cheng, H. M. Cheng, G. Q. Lu, *Chem. Commun.* **2009**, 1383–1385; b) Y. Z. Li, H. Zhang, X. L. Hu, X. J. Zhao, M. Han, *J. Phys. Chem. C* **2008**, *112*, 14973–14979; c) Q. Wang, C. C. Chen, W. H. Ma, H. Y. Zhu, J. C. Zhao, *Chem. Eur. J.* **2009**, *15*, 4765–4769; d) G. Liu, L. Z. Wang, C. H. Sun, X. X. Yan, X. W. Wang, Z. G. Chen, S. C. Smith, H. M. Cheng, G. Q. Lu, *Chem. Mater.* **2009**, *21*, 1266–1274.
[20] G. K. Mor, K. Shankar, M. Paulose, O. K. Varghese, C. A. Grimes, *Nano Lett.* **2006**, *6*, 215–218.
[21] a) J. M. Meichtry, M. Brusa, G. Mailhot, M. A. Grela, M. I. Litter, *Appl. Catal. B* **2007**, *71*, 101–107; b) P. Mohapatra, S. K. Samantaray, K. Parida, *J. Photochem. Photobiol. A* **2005**, *170*, 189–194.
[22] M. R. Hoffmann, S. T. Martin, W. Choi, W. Bahnemann, *Chem. Rev.* **1995**, *95*, 69–96.
[23] a) G. S. Li, D. Q. Zhang, J. C. Yu, *Environ. Sci. Technol.* **2009**, *43*, 7079–7085; b) I. C. Kang, Q. W. Zhang, S. Yin, T. Sato, F. Saito, *Environ. Sci. Technol.* **2008**, *42*, 3622–3626; c) T. Ohno, K. Sarukawa, K. Tokieda, M. Matsumura, *J. Catal.* **2003**, *213–220*, 82–86; d) P. Wang, B. B. Huang, Z. Z. Lou, X. Y. Zhang, X. Y. Qin, Y. Dai, Z. K. Zheng, X. N. Wang, *Chem. Eur. J.* **2010**, *16*, 538–544; e) Y. P. Bi, J. H. Ye, *Chem. Commun.* **2009**, 6551–6553.
[24] a) U.S. EPA, Chromium hexavalent (colorimetric), Vol Method 7196A, SW-846, Governmental Printing Office, **1992**; b) Y. C. Dai, G. R. Qian, Y. L. Cao, Y. Chi, Y. F. Xu, J. Z. Zhou, Q. Liu, Z. P. Xu, S. Z. Qiao, *J. Hazard. Mater.* **2009**, *170*, 1086–1092.

Received: December 8, 2009
Revised: March 13, 2010
Published online: July 19, 2010

